

Flight Data Assessment of Tightly-Coupled PPP/INS using Real-Time Products

Ryan Watson , Jason Gross, *West Virginia University*

Yoaz Bar-Sever, William Bertiger , Bruce Haines, *Jet Propulsion Laboratory*

Abstract—We present an analysis of the positioning performance of tightly-coupled Precise Point Positioning inertial navigation using two long-baseline flight data sets that include data from a navigation-grade Inertial Measurement Unit. The benefits of integrating inertial navigation with Precise Point Positioning are evaluated when using various GPS orbit and clock products (i.e., broadcast, real-time, and final), and whenever different troposphere models are adopted. We show that the positioning performance of PPP/INS, when using orbit and clock products generated in real-time is at the same level of accuracy as PPP when using post-processed orbit and clock products. In addition, we show that significant benefits with respect to solution convergence are available with tight-INS, leading to a greater than 30% reduction in three-dimensional (3D) Root Mean Squared (RMS) positioning errors. For example, when using real-time orbit and clock products with tightly-coupled inertial navigation, the mean and standard deviation of the position errors with respect to ambiguity-fixed post-processed reference solutions are reduced from 19 cm and 28 cm, to 15 and 18 cm, respectively. Furthermore, when using inertial data, a 10 cm or greater reduction in the 3D RMS position error is shown to be independent of the quality of the *a priori* nominal troposphere and troposphere modeling approach adopted.

Index Terms—Precise Point Positioning, Inertial Navigation, Tightly-Coupled Navigation, Real-Time PPP, Airborne Geodesy-Precise Point Positioning, Inertial Navigation, Tightly-Coupled Navigation, Real-Time PPP, Airborne Geodesy.

I. INTRODUCTION

Airborne geodetic techniques are superior to their terrestrial counterparts with respect to both economy and efficiency [1]. Additionally, airborne geodesy allows for mapping remote areas that would otherwise be inaccessible. A cornerstone for most airborne geodetic measurements is the accurate determination of the aircraft position and orientation. For this reason, airborne geodesy was not widely utilized until the advent of Global Navigation Satellite Systems (GNSS). Now – with precise GNSS positioning techniques – airborne geodesy is booming within several domains including: solid Earth monitoring (e.g., crustal deformation) [2]–[4], fluid Earth monitoring (e.g., ice sheet or sea-level monitoring) [5]–[7], and geoid determination [8], [9]. Despite the success of these airborne geodetic methods, the increased availability and reliability of accurate aircraft positioning remains an important enabling technology in support of future scientific endeavors.

Precise GNSS processing techniques can be broadly put into two categories: (1) single-receiver processing with undifferenced observations (i.e., Precise Point Positioning (PPP)), and (2) carrier-phase differential GNSS (CP-DGNSS) processing (e.g., Real Time Kinematic (RTK) or Network RTK

(NRTK)). CP-DGNSS processing strategies utilize additional static GNSS reference receivers to mitigate correlated error sources through cancellation by data differencing (e.g., atmospheric delays, ephemeris errors, and clock biases) [10], whereas PPP techniques rely on global correctors for the GNSS orbit and clocks along with models and dual-frequency data to mitigate these errors [11], [12].

The most common CP-DGNSS configuration is RTK, which consists of a single static GNSS reference receiver at a well-known location transmitting data to the roving platform so that double-differenced observables can be formed. This configuration works well for short-baseline separation between the mobile and reference receiver locations, and can readily produce centimeter-level positioning errors for airborne kinematic applications [13]–[15]; however, in this configuration, it is well-known that the positioning errors grow in proportion to the distance between the roving and reference receivers [16]. As such, RTK with successful integer ambiguity resolution is only feasible for a roughly 10 km radius around the reference receiver [10].

The maximum separation distance between the reference and roving receivers is greatly extended by using a network of static GNSS receivers, i.e., NRTK [17]. The NRTK approach allows for separations of approximately 100 km. However, it has recently been shown that NRTK network density spacing of less than 18 km is necessary to reduce network-side GNSS error-sources to a level that the roving receiver’s multipath errors are the dominant error-source [18]. Unfortunately, however, even the extended range of NRTK remains problematic for airborne sensing applications that can easily span 100s of km and oftentimes carry out missions in remote locations that do not have a dense GNSS reference network.

Another configuration, known as PPP-RTK, has been recently developed to leverage a network of static GNSS stations and extend upon the maximum baseline separation of RTK [19]. The PPP-RTK method resolves the carrier-phase ambiguities for the network, and provides that information in addition to precise orbit and clock information utilized by traditional PPP to accurately determine the platform’s position [20]. However, this positioning technique is subject to the same baseline limitation as NRTK.

To fully overcome the limitation imposed by requiring proximity to GNSS reference stations, the PPP processing strategy is the most promising precise GNSS processing technique for many specialized airborne geodetic applications. Several recent studies have shown that the accuracy of PPP

with respect to CP-DGNSS is comparable. For example, for static positioning, Colombo et al. show a 10 cm agreement, after PPP filter convergence [21]. Additionally, for kinematic applications, Honda et al. show decimeter-level positioning error agreement between RTK and PPP [22]. These studies show that PPP and RTK produce similar positioning accuracy after an initial convergence period of the PPP filter. This point was elaborated on by [23] where it is concluded that additional observations (e.g. multi-GNSS, inertial navigation) are needed to reduce the convergence period of PPP.

Recent attention has been focused on reducing the convergence period of PPP [24]. Of the techniques considered, the two most prevalent are: (a) leveraging the use of observations from multiple GNSS constellations [25], [26], and (b) integrating PPP with Inertial Navigation Systems (INS) [27]–[29]. While the RTGx supports multi-constellation GNSS data processing following the first consideration, this paper follows the second consideration and details the tight-integration INS within RTGx, and assesses its benefits for airborne kinematic applications.

This work is a significant extension of our work in [30] and [31]. In Watson (2016) [30], tight-integration of INS within PPP filters was conducted using simulated data in order to demonstrate exactly when and how much the incorporation of INS is beneficial for airborne kinematic PPP applications. In the simulation study, it was determined that INS is most important for accurate positioning when confronted with high-multipath, poor troposphere models, and low-quality GNSS orbit and clock products. Then, using recorded flight data provided by the National Geodetic Survey’s (NGS) Kinematic Processing Challenge, our work in Gross (2015) [31] validated the implementation of tightly-coupled INS models in JPL’s RTGx software by comparing PPP/INS and PPP filter solutions to post-processed reference PPP solutions.

In this article, the benefits of incorporating tight-INS in PPP filters when considering: (1) the accuracy (i.e., latency) of the orbit and clock products, and (2) the troposphere modeling approach are presented in order to offer insight to those considering the use of PPP for their particular application. First, a review of the details of tight-INS integration are presented. Next, two GPS/INS data sets recorded during long-baseline (i.e., ≥ 700 km) flights over Alaska are used to process PPP filters with and without the incorporation of tight-INS. Then the sensitivity of tight-INS benefits are shown when using: the GPS broadcast ephemeris, NASA’s Global Differential GNSS Service (GDGPS) real-time GNSS orbit and clock products, and JPL’s final post-processed orbit and clock products is considered. Finally, an assessment of the INS benefit sensitivity to troposphere modeling approaches is presented. A final contribution of this study is to share with the community that the JPL’s RTGx software incorporates a new tight-INS capability, so that it may be considered for use in airborne geodetic applications.

The rest of this article is organized in the following manner. The next section will provide background information on the processing software used in this study. Then the integration architecture and INS formulation will be covered. Finally, an analysis of flight data sets processed using varied ephemeris

and troposphere products is presented to demonstrate the benefits of tight-INS/PPP integration.

II. BACKGROUND

This section provides a short overview of the GNSS software tools and data products developed at JPL that are used in this study.

A. GIPSY-OASIS

JPL’s GNSS-Inferred Positioning System and Orbit Analysis Simulation Software package (GIPSY-OASIS) has been the primary geodetic and positioning software for several NASA missions: TOPEX/Poseidon [32], JASON [33], and GRACE [34] low Earth orbiting spacecraft. Additionally, it is operationally used to generate JPL’s precise GPS orbits and clock products [35]. GIPSY-OASIS is licensed for free by Caltech to academic institutions for research purposes.

B. JPL’s Global Differential GNSS System (GDGPS)

The Global Differential GPS (GDGPS) System is a GNSS monitoring and augmentation system that is composed of a large network of GNSS receivers and real-time processing software. Currently the real-time processing software is RTGx, which produces sub-decimeter real-time kinematic positioning for a large number of GNSS tracking sites, globally [www.gdgps.net].

C. RTGx

JPL’s new geodetic and navigation GNSS processing software, RTGx [36], is a redesign of JPL’s GIPSY-OASIS and Real-Time GIPSY software libraries and can be configured for real-time or post-processed GNSS orbit and clock determination, Low-Earth Orbiter (LEO) precise orbit determination, or PPP for both static and kinematic applications. RTGx supports multi-constellation GNSS and inherits unique features from the legacy GIPSY software, such as a single-receiver integer ambiguity resolution [37]. RTGx is operationally used with the GDGPS to generate real-time GNSS products, and it underlies the navigation software for the on-going development of the U.S. Air Force’s next generation GPS operational control segment (OCX) [38].

III. ALGORITHM FORMULATION

This section provides an overview of the PPP/INS integration architecture and a detailed discussion of the INS formulation currently utilized within RTGx. The PPP observation models will not be covered in this paper as they were not modified within RTGx for this study. For a review on the PPP observation models, the reader is referred to [11].

A. Integration Architecture

The integration of INS with GNSS is possible at different levels, namely: loosely-coupled, tightly-coupled or deeply-coupled [39]. In a loosely-coupled architecture, GNSS and INS are processed individually and then combined in a Kalman filter at the state-estimate-level. In a tightly-coupled architecture, INS estimates are used to model individual GNSS observables before combining in a single centralized estimation filter. These two integration methods have been used extensively for kinematic applications [27], [28], [40], where it has been shown that estimation performance is similar for both integration architectures for docile platforms, but the tightly-coupled architecture is known to have an advantage in more dynamic situations or situations with few GNSS observations. The deeply-coupled integration architecture utilizes the inertial information within the correlation process of the receiver's base-band processor [41]. This approach has the benefit of better tracking and re-acquisition of GNSS signals that are at reduced power levels [42]. However, deeply-coupled integration requires GNSS receiver modifications and is therefore not applicable for use in RTGx. As such, the tightly-coupled GNSS/INS architecture was adopted for integration in RTGx.

Schematically the tightly-coupled architecture is shown in Fig. 1, which depicts the estimation of GNSS observables, within the Kalman Filter (in our case RTGx uses a functionally equivalent Square Root Information Filter (SRIF)), using the inertial data and precise ephemeris information. The model predicts error-states using the difference between the INS predicted GNSS observables and the measured GNSS observables. For the PPP/INS filter's the estimated state vector is shown in Eq. 1, and is composed of:

- $\delta\Psi_{ib}$ - 3 INS attitude errors, where attitude is defined between the Earth-Centered-Inertial ECI (i) and aircraft body-axis (b) frames;
- δv^i - 3 INS velocity errors in ECI;
- δr^i - 3 INS position errors in ECI;
- b_a^b - 3 IMU tri-axial accelerometer sensor biases in the aircraft body-axis;
- b_g^b - 3 IMU tri-axial gyroscope sensor biases in the aircraft body-axis;
- δt_u - receiver clock bias;
- T_w - wet zenith tropospheric delay estimate;
- $N_{1\dots j}$ - GNSS carrier-phase bias estimates.

$$\mathbf{x} = \begin{pmatrix} \delta\Psi_{ib} \\ \delta v^i \\ \delta r^i \\ b_a^{accel} \\ b_b^{gyro} \\ \delta t_u \\ T_w \\ N_1 \\ \vdots \\ N_j \end{pmatrix} \quad (1)$$

An additional important aspect of tight-GNSS/INS depicted in Fig. 1 is the closed-loop nature of the system. In particular,

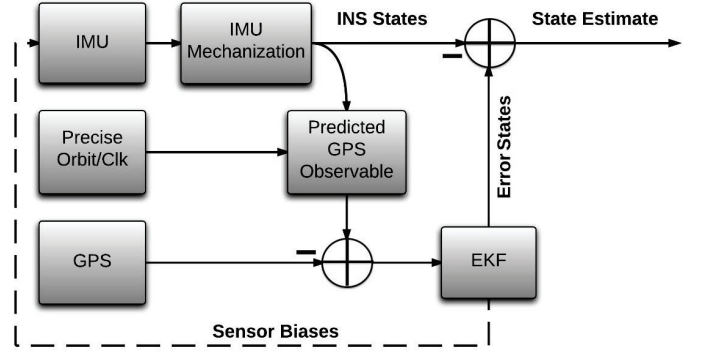


Fig. 1. Tightly-coupled GPS/INS integration schematic

the estimated IMU sensor biases are fed back to correct the raw IMU measurements in order to reduce the INS prediction errors. Furthermore, after each GNSS update, the position, velocity and attitude estimates determined by the INS are corrected by the estimated error-states. For the position and velocity estimates this is done with simple subtraction. For the attitude, small angle approximations are used to correct the INS estimates, as shown in Eq. 2

$$C_b^i = (I - \delta\Psi_{ib})\hat{C}_b^i, \quad (2)$$

where \hat{C}_b^i is the body-to-ECI direction cosine matrix (DCM) populated with the INS estimated attitude.

B. Inertial Navigation System Mechanization

As depicted in Fig. 2, the INS mechanization is comprised of three steps: attitude update, velocity update, and position update. This section summarizes the INS mechanization in the Earth-Centered Inertial (ECI) reference frame, which is offered in greater detail in numerous texts [39], [43]. The ECI INS mechanization was selected for implementation in RTGx, as ECI was already the frame used for assimilated data in RTGx's other applications (i.e., GNSS constellations, LEO satellites, etc.)

1) *Attitude Update*: To integrate attitude, a 3^{rd} -order Runge-Kutta integrator was used to propagate the platform's body-to-ECI quaternion [43], as shown in Eq. 3. Where I is an identity matrix, β is composed of the raw gyroscope measurements, as defined in Eq. 4, and the subscript t signifies the IMU time step (e.g., $t-2$ is using data from two discrete sample intervals in the past).

$$\hat{q}_t = [I + \frac{1}{12}(\hat{\beta}_t + 4\hat{\beta}_{t-1} + \hat{\beta}_{t-2}) + \frac{1}{12}(I + \frac{1}{4}\hat{\beta}_t)\hat{\beta}_{t-1}\hat{\beta}_{t-2} + \frac{1}{12}\hat{\beta}_t(\hat{\beta}_{t-1} - \frac{1}{2}\hat{\beta}_{t-2})]\hat{q}_{t-2} \quad (3)$$

With the 3rd-order integrator, attitude estimates are predicted at one-half the IMU data-rate (i.e., 200 Hz IMU data yields 100 Hz attitude estimates). The accumulation of integration and sensor errors can cause the integrated quaternion to lose

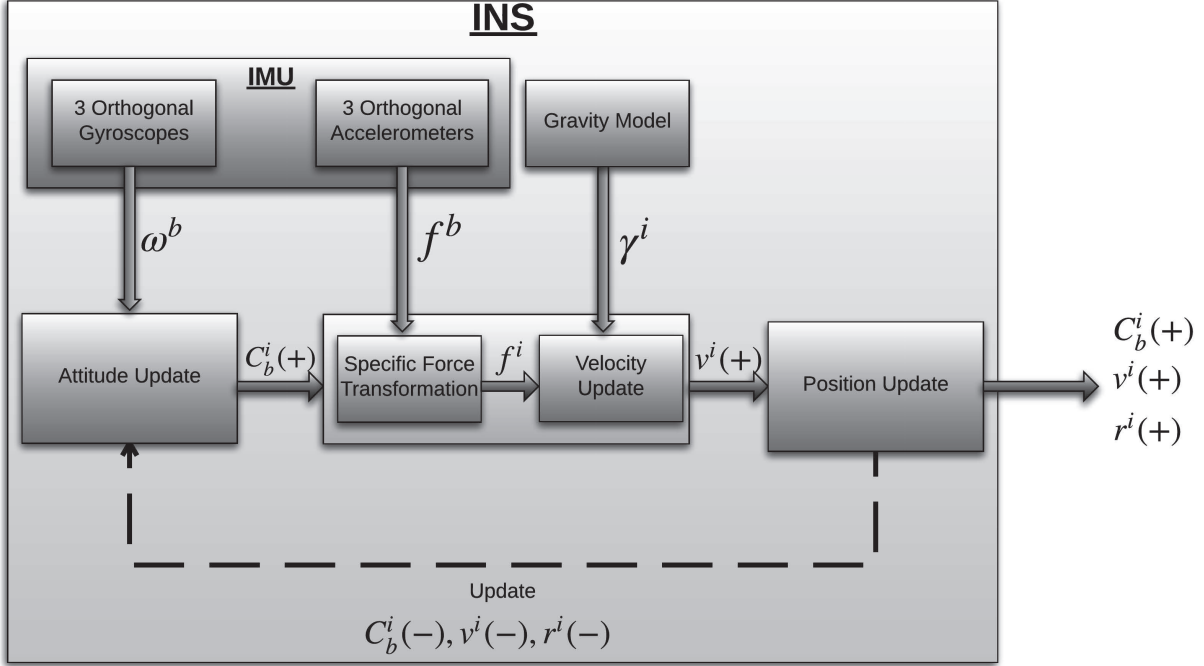


Fig. 2. Inertial navigation propagation schematic

$$\hat{\beta}_{t+1-n} = \begin{bmatrix} 0 & (3(\delta\theta_1)_{t+1-n} - (\delta\theta_1)_{t-n}) & (3(\delta\theta_2)_{t+1-n} - (\delta\theta_2)_{t-n}) & (3(\delta\theta_3)_{t+1-n} - (\delta\theta_3)_{t-n}) \\ (-3(\delta\theta_1)_{t+1-n} + (\delta\theta_1)_{t-n}) & 0 & (3(\delta\theta_3)_{t+1-n} - (\delta\theta_3)_{t-n}) & (-3(\delta\theta_2)_{t+1-n} + (\delta\theta_2)_{t-n}) \\ (-3(\delta\theta_2)_{t+1-n} + (\delta\theta_2)_{t-n}) & (-3(\delta\theta_3)_{t+1-n} + (\delta\theta_3)_{t-n}) & 0 & (3(\delta\theta_1)_{t+1-n} - (\delta\theta_1)_{t-n}) \\ (-3(\delta\theta_3)_{t+1-n} + (\delta\theta_3)_{t-n}) & (3(\delta\theta_2)_{t+1-n} - (\delta\theta_2)_{t-n}) & (-3(\delta\theta_1)_{t+1-n} + (\delta\theta_1)_{t-n}) & 0 \end{bmatrix} \quad (4)$$

its required orthonormality. To prevent this from happening, a periodic normalization of the quaternion was implemented.

2) *Velocity Update*: Using the updated INS attitude, the IMU specific force measurements are transformed from the body-frame to the ECI frame by multiplying with the the body-to-ECI DCM, C_b^i , as shown in Eq. 5, where the estimated body-to-ECI DCM is determined from the updated quaternion, using the relationships found in many texts [44]. approxiamatly

$$\Delta v^i = C_b^i \Delta v^b \quad (5)$$

With the specific force measurement transformed into the ECI reference frame, the velocity is calculated via Euler integration as shown in Eq. 6.

$$v_{k|k-1}^i = v_{k-1|k-1}^i + \Delta v^i + \gamma^i \tau \quad (6)$$

In Eq. 6, the updated INS velocity estimate is the summation of the previous velocity estimate ($k-1|k-1$) and the IMU measured change in velocity, Δv^i . Additionally, the component of acceleration that is due to the Earth's gravity in ECI, γ^i , must be modeled and integrated over the time-step, τ . For this application the Earth's gravity was modeled using the EGM-2008 gravity-field [45] out to degree and order 200.

3) *Position Update*: Finally, the position is updated from the previous position estimate via trapezoidal integration.

$$r_{k|k-1}^i = r_{k-1|k-1}^i + (v_{k|k-1}^i + v_{k-1|k-1}^i) \frac{\tau}{2} \quad (7)$$

While the estimation filter used in the study is realized in an ECI frame; for georeferencing applications, position must be known in an Earth Centered Earth Fixed (ECEF) frame. Therefore, in practice, before the estimated position and velocity are output to the end user, a position and velocity transformation from ECI to ECEF is conducted, which is based on the Earth's rotation rate, polar motion model, and time past which the ECI and ECEF frames were co-incident (i.e., typically the J2000 reference epoch) . The specific ECI-to-ECEF transformation realized within RTGx is the transformation adopted by the International Earth Rotation Service (IERS) [46].

C. Error-State Model

As discussed above, a portion of the estimated state vector consists of the INS error-states. As such, the dynamics of the INS error-states must also be modeled. From the error-state dynamic equations, a state transition matrix (STM) is formed via a power-series expansion of the Jacobian of the system of

equations in order to propagate the error-states from one time-step to another. This section will briefly review the elements of the INS error-state STM. For more details, comprehensive discussions of INS error-state models are offered by Groves (2013) [39] and Jekeli (2001) [43] on which the discussion herein is based upon.

1) *Attitude Error Propagation:* A small angle assumption is made when modeling the dynamics of the attitude errors. This allows the attitude error to be expressed as a vector of perturbations in the body frame with respect to the inertial frame, $\delta\Psi_{ib}^i$. If the attitude error is expressed as a DCM, then the error associated with the attitude is

$$[\delta\Psi_{ib\wedge}] \approx I_3 - \delta C_b^i, \quad (8)$$

where $[\delta\Psi_{ib\wedge}]$ represents the skew-symmetric matrix composed of small angle perturbations. The attitude error partial derivatives are calculated by differentiating the skew-symmetric matrix populated with the small angle perturbations.

$$[\delta\Psi_{ib\wedge}] \approx \delta C_b^i \quad (9)$$

Where the time derivative attitude error is

$$[\delta\dot{\Psi}_{ib\wedge}] \approx \tilde{C}_b^i \tilde{\Omega}_{ib}^b C_b^i + \tilde{C}_b^i C_b^i \Omega_{ib}^i, \quad (10)$$

which reduces to

$$\delta\dot{\Psi}_{ib} \approx \hat{C}_b^i b_b^{gyro}. \quad (11)$$

2) *Velocity Error Propagation:* In the Inertial frame, a body's acceleration is the summation of the specific force, measured by the accelerometer, and the gravitation acceleration, which must be modeled, as shown in Eq. 12.

$$a^i = \dot{v}^i = f^i + \gamma^i \quad (12)$$

Thus, taking the time derivative of Eq. 12 yields

$$\delta\dot{v}^i = \tilde{f}^i - f^i + \tilde{\gamma}^i - \gamma^i = \delta f^i - \delta \gamma^i, \quad (13)$$

which shows that the error associated with the derivative of the velocity in the Inertial frame are comprised of two parts: the error associated with the specific force (i.e., components 1 and 3 in the summation below), and the error associated with modeling the gravitation acceleration (i.e., component two in the summation below), as shown in Eq. 14.

$$\delta\dot{v}^i = -(\hat{C}_b^i \hat{f}^i) \delta\Psi_{ib} + \frac{2g}{r_{es}^e} \frac{\hat{r}^i}{|\hat{r}^i|^2} \hat{r}^{iT} \delta r^i + \hat{C}_b^i b_b^{accel} \quad (14)$$

In particular, due to the transformation of the IMU specific force measurements from the body-frame to ECI, the errors associated with the specific force in ECI is a combination of the accelerometer measurement errors (i.e., b_b^{accel}), in the body frame, and attitude errors (i.e., $\delta\Psi_{ib}$). Furthermore, in order to model the Earth gravity, the position in ECI must be known (i.e., δr^i).

3) *Position Error Propagation:* Finally, because the mechanization frame is ECI, the time-derivative of the position error is the velocity error.

$$\delta \dot{r}^i = \delta v^i \quad (15)$$

4) *Sensor Bias Dynamics:* For IMU accelerometer and rate gyroscope biases, the dynamics are modeled as first-order Gauss-Markov processes.

5) *System Dynamics and Transition Matrices:* Using the above defined error-state dynamics, the system matrix is defined in Eq. 16.

$$F_{INS}^i = \begin{bmatrix} 0_3 & 0_3 & 0_3 & 0_3 & \hat{C}_b^i \\ -(\hat{C}_b^i \hat{f}^i) & 0_3 & \frac{2g}{r_{es}^e} \frac{\hat{r}^i}{|\hat{r}^i|^2} \hat{r}^{iT} & \hat{C}_b^i & 0_3 \\ 0_3 & I_3 & 0_3 & 0_3 & 0_3 \\ 0_3 & 0_3 & 0_3 & 0_3 & 0_3 \\ 0_3 & 0_3 & 0_3 & 0_3 & 0_3 \end{bmatrix} \quad (16)$$

The system matrix, F, is used to calculate the discrete System Transformation Matrix (STM), Φ . The STM is calculated by taking the power series expansion, and for this study, a third-order expansion was used.

D. Practical Implementation Details

Beyond the INS mechanization, several practical implementation details are required for a proper design. This section overviews a few of these considered in the presented implementation.

1) *IMU to GNSS Lever Arm:* The above INS mechanization integrates the position and velocity at the location of the IMU. Therefore, the INS solution needs to be transposed to the same location as the GNSS solution (i.e. the phase center of the GNSS antenna) using Eq. 17,

$$r^{i,G} = r^{i,I} + \hat{C}_b^i L_b \quad (17)$$

where \hat{C}_b^i is the estimated platform attitude, the known lever-arm from the IMU to the GNSS antenna, L_b , represented in the platform's North, East, Down (NED) body-axis, and the superscripts G and I represent the GNSS antenna phase-center and IMU location, respectively. Similarly, the INS velocity solution must be transposed, as shown shown in Eq. 18: where Ω_{ib}^b is the skew-symmetric matrix of the IMU measured angular rate.

$$v_{k|k-1}^{i,G} = v^{i,I} + \hat{C}_b^i \Omega_{ib}^b L_b \quad (18)$$

This is done upon each GNSS measurement update, and reversed after the INS closed-loop feedback correction has been applied.

2) *GNSS and IMU Time-Alignment:* Another implementation issue is the precise time-tag alignment of the INS to the GNSS time-tag. This issue arises because the IMU measurements, although typically stamped with a GPS time-tag, are typically not scheduled to be precisely aligned with the GNSS measurement epochs. This means that IMU data must be used to predict the navigation states beyond the GNSS observation epoch and then linearly interpolated back to the time of the measurements. Furthermore, when a GNSS update occurs, an incremental error-state transformation matrix, which

provides the propagation mapping of INS error-states, must be used to map to the error-states to the GNSS measurement epoch. Then, after the GNSS update, the inverse of this transformation was used to map the predicted INS error-states back to the IMU time stamp in order to ensure that INS error-states remains consistent with the INS time-tags.

IV. ALGORITHM PERFORMANCE EVALUATION

A. Flight Data

Two flights tests of the National Oceanic and Atmospheric (NOAA) National Geodetic Survey (NGS) Gravity for the Re-definition of the American Vertical Datum (GRAV-D) project [47] that were flown over Alaska are used to conduct this study. In total, 6.3 hours of flight data are processed (i.e., 2.8 hours and 3.5 hours). The flight data sets consist of dual-frequency GPS pseudorange and carrier-phase observables recorded at 1Hz and an IMU's tri-axial accelerometer and rate gyroscope measurements recorded at a rate of 200 Hz. The commercial GNSS/INS system flown was a NovAtel SPAN system that is comprised of an OEM4-2G GPS receiver and a μ -IRS navigation-grade IMU. The surveyed lever-arm between the GPS antenna's phase-center and the IMU was provided by NOAA NGS, as well as the rotation angles relating the IMU's mounted orientation to the aircraft body-axis.

Fig. 3 shows the latitude/longitude flight profiles for the two flights processed in this study. The maximum range from the

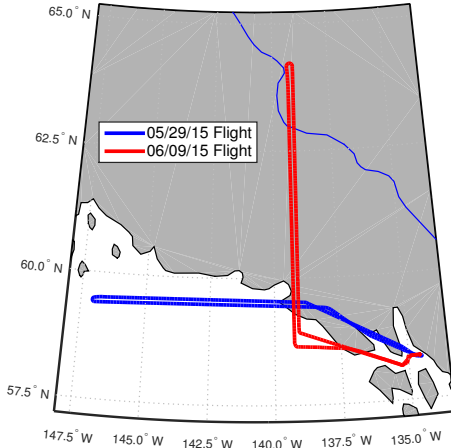


Fig. 3. Flight trajectories of the two GRAV-D GPS/INS data sets that were processed for this study

take-off location for the two flights was 727 km and 698 km respectively for the two flights, making the possibility of using RTK to single GNSS reference station impractical.

B. Reference Solution Strategy

The reference PPP position solutions were post-processed with JPL's GIPSY-OASIS II with JPL's Final orbit and clock products. In addition carrier-phase integer ambiguities were fixed by employing JPL's Wide-Lane Phase Bias products with their single receiver integer ambiguity resolution algorithm [37]. Finally, the position solutions were iterated

by making multiple passes over the data in which GNSS data-outliers were deleted from the final solution using an iterative windowing approach similar to the approach adopted by Gross (2016) [15]. With the iterative approach, once the position solution between successive data passes agreed to the centimeter-level, the solution was accepted as final. The reference attitude solutions used in the error analysis are the filtered and smoothed solutions reported NovAtel SPAN post-processing software.

For this study, all the error comparisons are drawn with respect to forward-filter solutions, as would be employed for real-time applications. That is, the need for rapid convergence only applies to real-time applications, as PPP solution convergence is not a problem for post-processing estimators that employ a backward pass through the data with a Kalman smoother. Additionally, throughout this error analysis, the estimation performance evaluation of the PPP filters is only conducted whenever the airplane was at its science cruise altitude. The primary reason for starting the error comparisons at altitude is due to the fact that post-processed PPP reference solutions are known to have the largest solution uncertainty during the flight's ascent and decent periods, whenever the tropospheric delay is rapidly changing and cannot easily be distinguished from the vertical positioning error. Therefore, by eliminating these periods from the error-analysis, and instead using the solutions only at altitude, where the troposphere delays can be tightly constrained to an input model, the periods in which the reference solutions are expected to exhibit their largest uncertainty cannot skew the error analysis. Furthermore, as most airborne geodetic applications are only concerned with the positioning accuracy during the portion of the flight when the scientific instrumentation is active at altitude, if the solution is lost during this period due to a large bank, etc., the rapid convergence obtained with INS would help maintain accuracy.

C. Real-Time Processing Strategy

The dual-frequency ionosphere-free pseudorange and carrier-phase data combinations were used for all filters. The measurement noise assumed on every pseudorange and carrier-phase dual-frequency observable was 2.5 meters and 2.5 mm, respectively. The filter utilized by RTGx is formulated as a generalized Square-Root Information Filter (SRIF) [48]. This formulation allows any modeled parameter to be estimated as a first-order Gauss-Markov stochastic process (i.e. ranging from white-noise to random-walk). Table I lists the stochastic models used for each of the PPP and INS model parameters for the filters evaluated in this study.

For filter efficiency, we elected to perform system process noise updates at 1 Hz (i.e., the same rate as the GNSS data). However, because 1 second update intervals are much longer than the 100 Hz INS integration intervals, the INS process noise becomes correlated amongst the navigation states (i.e., off diagonal terms exist). Fortunately, this correlation can be analytically propagated [39]. However, in this study, for simplicity, standard uncorrelated process noise updates were used, and to arrive at the values listed in Table I, the IMU

TABLE I
SELECTED STOCHASTIC MODELS PARAMETERS FOR PPP AND PPP/INS FILTERS

Parameter	Only with INS	<i>a priori</i> σ	Process Noise	Correlation Time
Position	No	0.5 m	$5 \frac{m}{\sqrt{s}}$	∞
Trop. Wet Zenith Delay	No	0.05 m	$5e-7 \frac{m}{\sqrt{s}}$	∞
Receiver Clock	No	1000 m	$1000 \frac{m}{\sqrt{s}}$	0
Phase Biases	No	3e8 m	$0 \frac{m}{\sqrt{s}}$	∞
Velocity	Yes	2.0 m/s	$0.28e-3 \frac{m}{\sqrt{s}}$	∞
Attitude	Yes	5.0 deg.	$4e-5 \frac{deg.}{\sqrt{s}}$	∞
Accelerometer Biases	Yes	0.05 $\frac{m}{s^2}$	$0.263e-4 \frac{m}{\sqrt{s}}$	∞
Gyroscope Biases	Yes	2.8 deg./s	$4e-5 \frac{deg./s}{\sqrt{s}}$	∞

stochastic model parameters were initially assigned based on the expected range for a navigation grade IMU provided by [39] and empirical tuning was used increase them to account for the 1 Hz update interval and optimize the positioning performance.

V. RESULTS AND DISCUSSION

A. Positioning Performance

1) *Sensitivity to Orbit/Clock Products*: For this sensitivity study, although all of the filters were run in forward filter only as a real-time estimator, in order to assess the sensitivity to orbit/clock product quality, the use of final post-processed GPS orbit/clock products were used (i.e., knowing that final orbits/clocks that are post-processed could never be used in real-time) in addition to real-time orbits/clocks and the GPS broadcast ephemeris. This was conducted in order to assess the impact of the quality of the orbit/clock products with respect to the benefits of tightly-coupled PPP/INS.

The positioning performance when using broadcast orbit/clock products both with INS and without is depicted in Fig. 4, in which the cumulative distribution function (CDF) of the residual sum of squares (RSOS) for both forward-filter-only shows the overall positioning error reduction due to the incorporation of INS. This is also shown in Table II, where the INS solution is shown to yield approximately a 30 cm reduction with respect to position mean, standard deviation, and RMS errors.

The sensitivity of the positioning performance when using real-time and final orbit/clock products is shown in Fig. 5, where it should be noted that there is approximately a 1 meter error reduction with respect to positioning performance obtained using broadcast products. One of the most notable insights drawn from Table II is that the PPP/INS using real-time products outperforms the PPP filter even when using final orbits/clock products with respect to RMS and standard deviation errors. This is significant because it suggests that INS reduces the latency needed to produce the highest quality positioning performance. Furthermore, it is also apparent that the GPS-only PPP solutions with real-time and final products are largely equivalent (i.e., within a cm for most metrics), but that there is an additional 2-3 cm error reduction with respect to metrics reported in Table II when comparing the PPP/INS solutions that use real-time products and final products. This

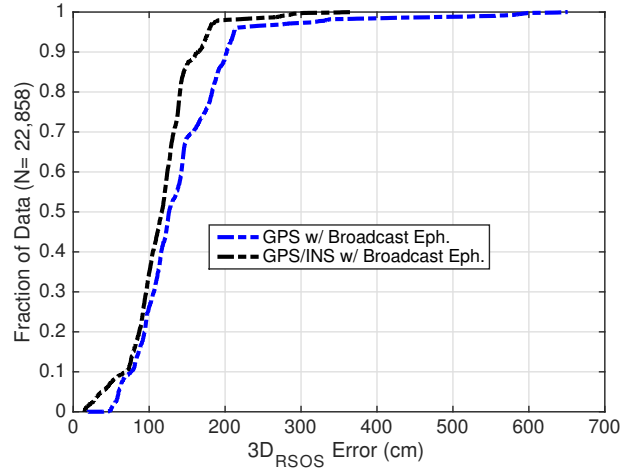


Fig. 4. Cumulative distribution of $3DR_{SOS}$ positioning error of the forward-filter GPS solutions with and without including INS. Both solutions are processed using the PPP models in RTGx, but with the Broadcast GPS orbit and clock solutions.

suggests that is is beneficial to use INS even when final orbits are available.

TABLE II
POSITIONING ERROR STATISTICS FOR TWO ALASKAN FLIGHTS.

$3DR_{SOS}$ (cm)	Median	μ	σ	RMS	Max.
GPS _{Brdc}	128.6	141.8	71.9	159.0	651.1
GPS/INS _{Brdc}	115.6	114.7	42.05	122.2	369.8
PPP _{RT}	11.3	19.1	27.9	33.8	312.8
PPP/INS _{RT}	11.2	15.3	17.6	23.3	227.0
PPP _{Final}	10.9	19.4	28.9	34.7	297.5
PPP/INS _{Final}	9.2	13.8	13.8	19.5	235.4

2) *Convergence Improvements with INS*: The clearest benefit of tight-INS integration within PPP is the reduction of the solution convergence time. This is depicted with respect to estimated states in Figs. 6, 7 and 8. Fig. 6 shows a substantial benefit of INS integration with respect to positioning during the first half-hour of the real-time PPP solution.

In Fig. 6 the tight-INS PPP filter converges to less than 10 cm errors within a few minutes, where as the GPS-only PPP filters takes nearly one-half hour. The convergence benefit is also shown in Fig. 7, which shows convergence of the carrier-phase bias estimates during the first 15-minutes of the forward-

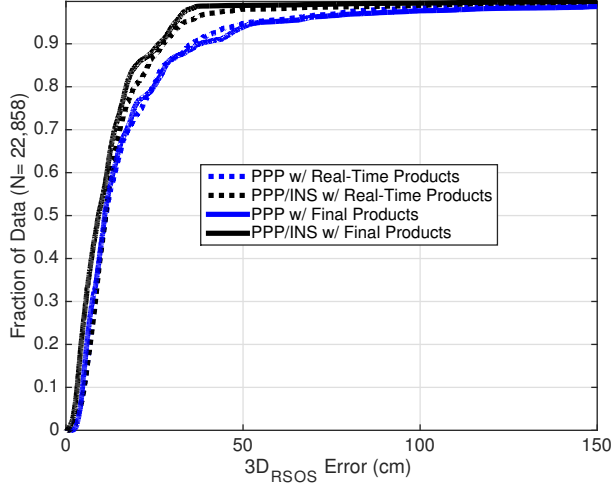


Fig. 5. Cumulative distribution of $3D_{RSOS}$ positioning error of the forward-filter PPP solutions with and without including INS. Solutions that use both GDGPS real-time and the JPL's IGS final GPS orbit and clock products are shown.

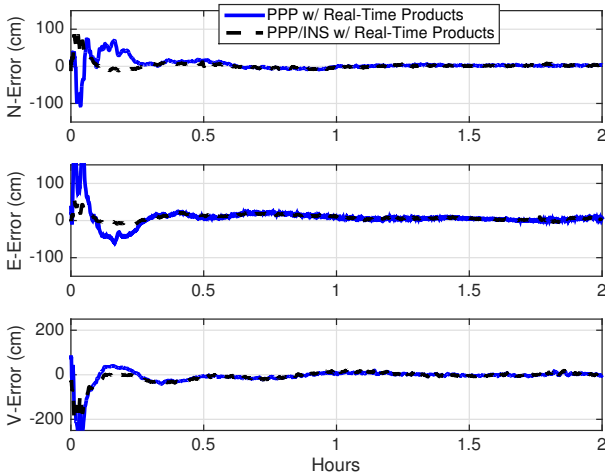


Fig. 6. Example of convergence benefit of INS integration during the half hour of the real-time PPP solution when compared to the post-processed ambiguity-fixed PPP reference solution.

filter solution.

In Fig. 7, phase-bias errors for each of the satellites tracked at the start of the data set are estimated with respect to their final steady-state estimates. For each satellite, the tight-INS solution consistently enhances that filter's ability to quickly converge upon the carrier-phase bias. Fig. 8 shows an example of troposphere zenith delay estimation error convergence during the first 15-minutes of the filter that used real-time products with and without tight-INS integration. The errors are calculated with respect to the Vienna Mapping Function (VMF) [49] Grid delay estimation, which shows that the integrated solution converges to the correct troposphere delay in a more stable manner when compared to the solution without INS.

Finally, when comparing positioning performance after a

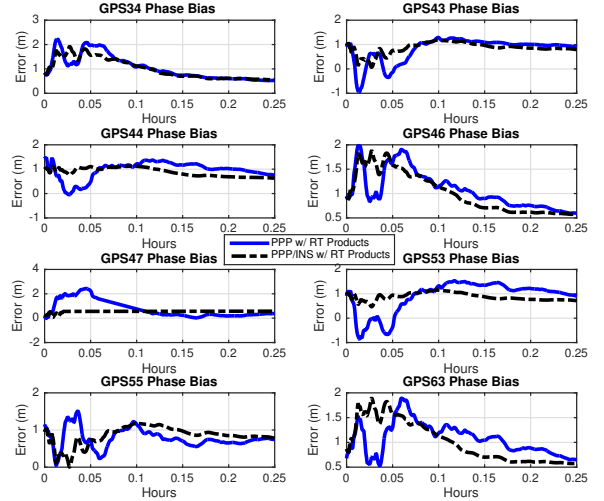


Fig. 7. Example of GPS carrier-phase biases converging during the first 15-minutes of the Real-Time filter with and without INS integration. Phase bias errors are estimated with respect to their final estimated steady-state values at 3.5 hours into the flight.

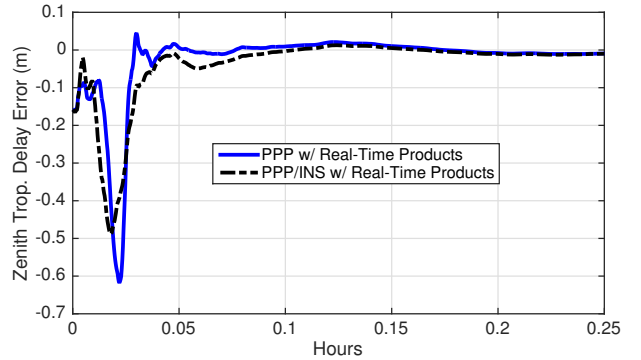


Fig. 8. Example of troposphere zenith delay estimation error convergence during the first 15-minutes of the Real-Time filter with and without INS integration. Errors are estimated with respect to Vienna Mapping Function (VMF) Grid delay estimation generated by accepting the position solution of the post-processes ambiguity-fixed PPP reference.

30-minute convergence, as shown in Table III, it becomes apparent that the positioning estimation performance is nearly identical between the filters with and without INS. This further substantiates that INS primary benefit is to reduce the PPP solutions initial convergence.

TABLE III
POSITIONING ERROR STATISTICS WITH REAL-TIME ORBIT AND CLOCK PRODUCTS FOR TWO ALASKAN FLIGHTS AFTER A 30-MINUTE FILTER CONVERGENCE PERIOD.

$3D_{RSOS}$ (cm)	Median	μ	σ	RMS	Max.
PPP _{RT}	9.7	11.3	7.6	13.2	43.2
PPP/INS _{RT}	9.2	11.3	6.8	13.6	43.6

3) *Sensitivity to Troposphere Nominal and Mapping Function*: To evaluate the positioning performance with respect to the method utilized to model the troposphere, four different

troposphere modeling approaches were adopted, including: (1) a low-fidelity approach in which no wet or dry nominal delay was provided to the filter, (2) a standard approach in which a scale height was used to model the dry delay and the wet delay is estimates, and (3) and (4) post-processing approaches in which both wet and dry delays are provided based on reference products. In each case, the positioning error sensitivity to the troposphere nominal and model are summarized in Table IV. From Table IV, a 10 cm reduction in both standard deviation

TABLE IV
POSITIONING ERROR SENSITIVITY TO TROPOSPHERE NOMINAL MODEL AND MAPPING FUNCTIONS. ALL FILTERS USE REAL-TIME ORBITS AND CLOCKS.

3DRSOS (cm)	Median	μ	σ	RMS	Max.
PPP _{No Nom., Neill}	38.4	43.8	31.6	54.0	394.7
PPP/INS _{No Nom., Neill}	35.1	36.4	21.2	42.1	262.4
PPP _{Static Nom., Neill}	11.3	19.1	27.9	33.8	312.8
PPP/INS _{Static Nom., Neill}	11.2	15.3	17.6	23.3	227.0
PPP _{GPT2 Nom., GMF}	10.8	19.5	28.2	34.3	306.4
PPP/INS _{GPT2 Nom., GMF}	11.2	16.0	18.0	24.0	254.4
PPP _{VMF1 Nom., VMF1}	11.2	18.6	28.1	33.7	306.1
PPP/INS _{VMF1 Nom., VMF1}	11.2	14.6	17.6	22.9	266.5

and RMS positioning error due to INS integration regardless of the troposphere nominal and modeling approach. This suggests that the INS enables better separation of position estimates from the troposphere delay.

B. Attitude Estimation

An important benefit of INS is the availability of an attitude solution, which is not present with only GPS. Table V shows good agreement of the RTGx/INS attitude solution with respect to the attitude provided by the NovAtel SPAN system.

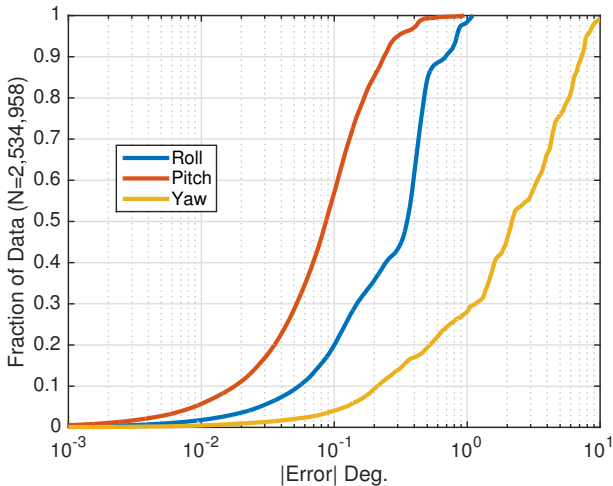


Fig. 9. Cumulative distribution of attitude error of the real-time forward-filter PPP solutions with INS. Errors are calculated with respect to the on-board real-time NovAtel SPAN estimates as a reference solution

From both Table V and Fig. 9, the heading error is noticeably larger than the roll and pitch errors. This is expected due to the nature of the flight. Each data set contains almost entirely long periods straight and level flight. During these

flight conditions, it is well-known that IMU yaw biases have issues with respect to observability [50].

TABLE V
ATTITUDE ERROR STATISTICS FOR TWO GRAV-D ALASKA FLIGHTS. ERRORS ARE CALCULATED WITH RESPECT TO THE ON-BOARD REAL-TIME NOVATEL SPAN ESTIMATES AS A REFERENCE.

Error (deg.)	Median	μ	σ	Max.
ϕ	0.35	0.33	0.24	1.10
θ	0.09	0.11	0.10	0.95
ψ	2.17	3.10	2.70	15.61

VI. CONCLUSIONS

For airborne geodetic applications that need accurate positioning, require long-baseline flights, and are flying in locations that are distant from a dense GNSS ground reference station network, the PPP processing technique is favorable over RTK or NRTK. However, for use in real-time applications, it is well known that PPP, when compared to RTK, is slower to converge to accurate positioning. This slow convergence property may become an issue in real-time if the solutions is intermittently lost mid-flight due to the loss of carrier-phase lock, which may occur, for example, during a large aircraft bank. As such, the performance and sensitivity of tightly-coupled PPP/INS has been presented using two long-baseline flight data sets in order to demonstrate the benefits of tight-INS with respect to improving the convergence properties of real-time PPP. In particular, the integrated INS solutions have been shown to speed up convergence, leading to a reduction in positioning error that exceeds 30%. Furthermore, the improved solution convergence offered by tight-INS has also been demonstrated by comparing the real-time estimated zenith tropospheric delay to a post-processed reference, and by comparing the real-time estimated carrier-phase biases to their estimated steady-state values.

To offer additional insight, this paper has also presented the sensitivity of the benefit of using tightly-coupled PPP/INS while other typical PPP error sources are reduced through other means. For example, the sensitivity of PPP/INS when using various latency GPS orbit and clock products (i.e., GPS broadcast orbits/clocks, real-time GDGPS orbits/clocks, and JPL final post-processed GPS orbits/clocks) has been presented. From this sensitivity study, it has been shown that a tight-PPP/INS filters that use real-time GNSS orbit/clock products, which are known to have cm-to-dm-level errors with respect to final orbit/clock products, is able to outperform the positioning solutions that are based upon GPS-only PPP that use final post-processed orbit/clock products. Additionally, a similar sensitivity study has been presented with respect to the fidelity of the PPP filter's tropospheric delay modeling approach. In this case, it has been demonstrated that the benefit of tightly-coupled INS remains consistent, irrespective of the fidelity of tropospheric delay estimation approach that is adopted.

In summary, for airborne applications that require accurate real-time solutions and robustness to signal outages, cycle-slips, etc., tightly-coupled INS is an important way to compensate for the slow convergence properties of real-time PPP, and

this benefit remains important even as other PPP error sources, namely, orbit/clock errors and tropospheric delay errors, are reduced.

ACKNOWLEDGMENT

This work was supported through a subcontract with the California Institute of Technology Jet Propulsion Laboratory. The authors would like to thank the NOAA National Geodetic Survey for providing the flight data sets.

REFERENCES

- [1] C. Glennie, "An analysis of airborne gravity by strapdown dgps/ins," Master's thesis, University of Calgary, March 1999.
- [2] P. Rosen, S. Hensley, K. Wheeler, and G. Sadowy, "Uavsar: a new nasa airborne sar system for science and technology research," *IEEE Conference on Radar*, 2006.
- [3] P. Prats, A. Reigber, J. J. Mallorquí, R. Scheiber, and A. Moreira, "Estimation of the temporal evolution of the deformation using airborne differential sar interferometry," *IEEE Transactions on Geoscience and Remote Sensing*, vol. 46, no. 4, pp. 1065–1078, 2008.
- [4] C. Glennie, W. Carter, R. Shrestha, and D. WE, "Geodetic imaging with airborne lidar: the earth's surface revealed," *Reports on Progress in Physics*, vol. 76, no. 8, 2013.
- [5] K. Mattar, P. Vachon, D. Geudtner, and G. AL, "Validation of alpine glacier velocity measurements using ers tandem-mission sar data," *IEEE Transactions on Geoscience and Remote Sensing*, vol. 36, no. 3, pp. 974–984, 1998.
- [6] C. Richez, "Airborne synthetic aperture radar tracking of internal waves in the strait of gibraltar," *Progress in Oceanography*, vol. 33, no. 2, pp. 93–159, 1994.
- [7] J. C. Brock, W. C.W., A. Sallenger, W. Krabill, and S. R.N., "Basis and methods of nasa airborne topographic mapper lidar surveys for coastal studies, journal of coastal research," *Journal of Coastal Research*, vol. 18, pp. 1–13, 2002.
- [8] R. Forsberg, A. Olesen, L. Bastos, A. Gidskehaug, U. Meyer, and L. Timmen, "Airborne geoid determination," *Earth, Planets and Space*, vol. 52, 2000.
- [9] P. Novak, M. Kern, K. Schwarz, S. M.G., B. Heck, S. Ferguson, Y. Hammada, and M. Wei, "On geoid determination from airborne gravity," *Journal of Geodesy*, vol. 76, 2003.
- [10] P. Misra and P. Enge, *Global Positioning System: Signals, Measurements and Performance Second Edition*. Lincoln, MA: Ganga-Jamuna Press, 2006.
- [11] J. Zumberge, M. Heflin, D. Jefferson, M. Watkins, and F. Webb, "Precise point positioning for the efficient and robust analysis of gps data from large networks," *Journal of Geophysical Research: Solid Earth (1978–2012)*, vol. 102, no. B3, pp. 5005–5017, 1997.
- [12] J. Kouba and P. Héroux, "Precise point positioning using igs orbit and clock products," *GPS solutions*, vol. 5, no. 2, pp. 12–28, 2001.
- [13] C. Eling, L. Klingbeil, and H. Kuhlmann, "Development of an rtk-gps system for precise real-time positioning of lightweight uavs." *Ingenieurvermessungskurs*, 2014, pp. 243–254.
- [14] H. Bendea, P. Boccardo, S. Dequal, F. Giulio, D. Marenchino, and M. Piras, "Low cost uav for post-disaster assessment," *Int. Archives of Photogrammetry, Remote Sensing and Spatial Information Sciences*, 2008.
- [15] J. Gross, R. Watson, S. D'Urso, and Y. Gu, "Flight-test evaluation of kinematic precise point positioning of small uavs," *International Journal of Aerospace Engineering*, 2016.
- [16] N. Brown, R. Keenan, B. Richter, and L. Troyer, "Advances in ambiguity resolution for rtk applications using the new rtm v3.0 master auxiliary messages." ION GNSS, 2005.
- [17] U. Vollath, H. Landau, X. Chen, K. Doucet, and C. Pagle, "Network rtk versus single base rtk - understanding the error characteristics." ION GNSS, 2002.
- [18] M. J. Murrian, C. W. Gonzalez, T. E. Humphreys, and T. D. Novlan, "A dense reference network for mass-market centimeter-accurate positioning," in *2016 IEEE/ION Position, Location and Navigation Symposium (PLANS)*. IEEE, 2016, pp. 243–254.
- [19] G. Wübbena, M. Schmitz, and A. Bagge, "Ppp-rtk: precise point positioning using state-space representation in rtk networks," in *Proceedings of ION GNSS*, vol. 5, 2005, pp. 13–16.
- [20] P. Teunissen and A. Khodabandeh, "Review and principles of ppp-rtk methods," *Journal of Geodesy*, 2014.
- [21] O. Colombo and A. Evans, "Evaluation of precise, kinematic gps point positioning." ION GNSS, 2004, pp. 217–222.
- [22] M. Honda, M. Murata, and Y. Mizukura, "Development and assessment of gps precise point positioning software for land vehicular navigation," vol. 6, 2007.
- [23] S. Bisnath and Y. Gao, "Current state of precise point positioning and future prospects and limitations," in *Observing our changing earth*. Springer, 2009, pp. 615–623.
- [24] C. Rizos, V. Janssen, C. Roberts, and T. Grinter, "Precise point positioning: Is the era of differential gnss positioning drawing to an end?" 2012.
- [25] C. Cai, Y. Gao, L. Pan, and J. Zhu, "Precise point positioning with quad-constellations: Gps, beidou, glonass and galileo," *Advances in Space Research*, vol. 56, no. 1, pp. 133–143, 2015.
- [26] X. Ren, S. Choy, K. Harima, and X. Zhang, "Multi-constellation gnss precise point positioning using gps, glonass and beidou in australia," in *International Global Navigation Satellite Systems (IGNSS) Symposium*. International Global Navigation Satellite Systems Society, 2015, pp. 1–13.
- [27] S. Du, "Integration of precise point positioning and low cost mems imu," Master's thesis, University of Calgary, November 2010.
- [28] N. S. Kjørsvik, J. G. O. Gjevestad, E. Broste, K. Gade, and O.-K. Hagen, "Tightly coupled precise point positioning and inertial navigation systems," in *International Society for Photogrammetry and Remote Sensing European Calibration and Orientation Workshop*. IPRS, 2010.
- [29] M. A. Rabbou and A. El-Rabbany, "Tightly coupled integration of gps precise point positioning and mems-based inertial systems," *GPS Solutions*, vol. 19, no. 4, pp. 601–609, 2015.
- [30] R. Watson, V. Sivaneri, and J. Gross, "Performance Characterization of Tightly-Coupled GNSS Precise Point Positioning Inertial Navigation within a Simulation Environment," in *Submitted to the 2016 AIAA Guidance Navigation and Control Conference*. AIAA, 2016.
- [31] J. Gross, R. Watson, V. Sivaneri, Y. Bar-Sever, W. Bertiger, and B. Haines, "Integration of inertial navigation into real-time gipsy-x (rtgx)," in *Proceedings of the 28th International Technical Meeting of The Satellite Division of the Institute of Navigation (ION GNSS+ 2015)*, Tampa, FL, 2015.
- [32] T. Yunck, W. Bertiger, S. Wu, Y. Bar-Sever, E. Christensen, B. Haines, S. Lichten, R. Muellerschoen, Y. Vigue, and P. Willis, "First assessment of gps-based reduced dynamic orbit determination on topex/poseidon," *Geophysical research letters*, vol. 21, no. 7, pp. 541–544, 1994.
- [33] B. Haines, Y. Bar-Sever, W. Bertiger, S. Desai, and P. Willis, "One-centimeter orbit determination for jason-1: new gps-based strategies," *Marine Geodesy*, vol. 27, no. 1-2, pp. 299–318, 2004.
- [34] R. Kroes, O. Montenbruck, W. Bertiger, and P. Visser, "Precise grace baseline determination using gps," *GPS Solutions*, vol. 9, no. 1, pp. 21–31, 2005.
- [35] S. Desai, W. Bertiger, J. Gross, B. Haines, N. Harvey, C. Selle, A. Sibthorpe, and J. Weiss, "Results from the reanalysis of global gps data in the igs08 reference frame," 2011.
- [36] Y. E. Bar-Sever, W. I. Bertiger, A. R. Dorsey, N. E. Harvey, W. Lu, K. J. Miller, M. A. Miller, L. J. Romans, A. J. Sibthorpe, J. P. Weiss, M. Garcia-Fernandez, and J. Gross, "Real-time and post-processed orbit determination and positioning, U.S. Patent No. 9,057,780 B2," Jun. 18 2015.
- [37] W. Bertiger, S. D. Desai, B. Haines, N. Harvey, A. W. Moore, S. Owen, and J. P. Weiss, "Single receiver phase ambiguity resolution with gps data," *Journal of Geodesy*, vol. 84, no. 5, pp. 327–337, 2010.
- [38] W. Bertiger, Y. Bar-Sever, E. Bokor, M. Butala, A. Dorsey, J. Gross, N. Harvey, W. Lu, K. Miller, M. Miller *et al.*, "First orbit determination performance assessment for the OCX navigation software in an operational environment," in *Proceedings of the 25th International Technical Meeting of The Satellite Division of the Institute of Navigation (ION GNSS+ 2012)*, 2012.
- [39] P. D. Groves, *Principles of GNSS, inertial, and multisensor integrated navigation systems*. Artech House, 2013.
- [40] S. Du and Y. Gao, "Inertial aided cycle slip detection and identification for integrated ppp gps and ins," *Sensors*, vol. 12, no. 11, pp. 14344–14362, 2012.
- [41] A. Soloviev, F. Graas, and G. Sanjeev, "Implementation of deeply integrated gps/low-cost imu for reacquisition and tracking of low cnr gps signals," in *National Technical Meeting of The Institute of Navigation*, 2004.
- [42] G. Goa and G. Lachapelle, "A novel architecture for ultra-tight hsgps-ins integration," *Journal of Global Positioning Systems*, vol. 7, 2008.

- [43] C. Jekeli, *Inertial navigation systems with geodetic applications*. Walter de Gruyter, 2001.
- [44] B. L. Stevens and F. L. Lewis, *Aircraft control and simulation*. John Wiley & Sons, 2003.
- [45] N. K. Pavlis, S. A. Holmes, S. C. Kenyon, and J. K. Factor, "An earth gravitational model to degree 2160: Egm2008," *EGU General Assembly*, pp. 13–18, 2008.
- [46] G. Petit and B. Luzum, Eds., *IERS Conventions (2010)*, (*IERS Technical Note ; 36*).
- [47] T. M. Damiani, A. Bilich, and G. L. Mader, "Evaluating Aircraft Positioning Methods for Airborne Gravimetry: First Results from GRAV-D's Kinematic GPS Processing Challenge," in *Proceedings of the 26th International Technical Meeting of The Satellite Division of the Institute of Navigation (ION GNSS+ 2013)*, 2013.
- [48] G. J. Bierman, *Factorization methods for discrete sequential estimation*. Courier Corporation, 2006.
- [49] J. Boehm, B. Werl, and H. Schuh, "Troposphere mapping function for gps and very long baseline interferometry from european centre for medium-range weather forecasts operational analysis data," *Journal of Geophysical Research*, 2006.
- [50] D. Becker, M. Becker, S. Leinen, and Y. Zhao, "Estimability in strap-down airborne vector gravimetry," 2015.